Structure and Specificity of a Quorum-Quenching Lactonase (AiiB) from *Agrobacterium tumefaciens*[†,‡]

Dali Liu,[§,||] Pei W. Thomas,[||,⊥] Jessica Momb,[#] Quyen Q. Hoang,[§] Gregory A. Petsko,[§] Dagmar Ringe,*[,§] and Walter Fast*[,⊥,#,▽]

Division of Medicinal Chemistry, College of Pharmacy, the Graduate Program in Biochemistry, and the Texas Institute for Drug and Diagnostic Development at The University of Texas, Austin, Texas 78712, and Departments of Chemistry and Biochemistry and Rosenstiel Basic Medical Sciences Research Center, Brandeis University, Waltham, Massachusetts 02454-9110

Received June 29, 2007; Revised Manuscript Received August 6, 2007

ABSTRACT: *N*-Acyl-L-homoserine lactone (AHL) mediated quorum-sensing regulates virulence factor production in a variety of Gram-negative bacteria. Proteins capable of degrading these autoinducers have been called "quorum-quenching" enzymes, can block many quorum-sensing dependent phenotypes, and represent potentially useful reagents for clinical, agricultural, and industrial applications. The most characterized quorum-quenching enzymes to date are the AHL lactonases, which are metalloproteins that belong to the metallo-beta-lactamase superfamily. Here, we report the cloning, heterologous expression, purification, metal content, substrate specificity, and three-dimensional structure of AiiB, an AHL lactonase from *Agrobacterium tumefaciens*. Much like a homologous AHL lactonase from *Bacillus thuringiensis*, AiiB appears to be a metal-dependent AHL lactonase with broad specificity. A phosphate dianion is bound to the dinuclear zinc site and the active-site structure suggests specific mechanistic roles for an active site tyrosine and aspartate. To our knowledge, this is the second representative structure of an AHL lactonase and the first of an AHL lactonase from a microorganism that also produces AHL autoinducers. This work should help elucidate the hydrolytic ring-opening mechanism of this family of enzymes and also facilitate the design of more effective quorum-quenching catalysts.

Various Gram-negative bacteria rely on production and detection of *N*-acyl-L-homoserine lactone (AHL)[1] autoinducers for regulating cell-density dependent behavior (*1*). Methods to disrupt quorum-sensing in these bacteria are of significant interest for clinical, agricultural, and industrial applications (*2*). Some of the most effective "quorum-quenching" agents reported to date are enzymes capable of catalyzing hydrolytic lactone ring opening (*3*, *4*). With the exception of a recently reported phosphotriesterase homologue (*5*) and the relatively inefficient human paroxonases (*6*), most of these AHL lactonases show significant sequence and structural homology to the metallo-β-lactamase superfamily (*7*). Despite potential applications, the structure and specificity of only one AHL lactonase, AiiA (autoinducer inactivation gene product) from *Bacillus thuringiensis*, has been extensively characterized to date (*8*, *9*). Because *Bacillus* species do not use AHL-dependent quorum-sensing, there is some debate about the true physiological function of AiiA (*10*). Also, many questions remain about the catalytic mechanism of AHL lactonases in general. These concerns highlight the need to study quorum-quenching catalysts derived from organisms known to use AHL signaling.

[†] This research was supported in part by the Texas Advanced Research Program (003658-0018-2006 to W.F.), the Robert A. Welch Foundation (F-1572 to W.F.), and National Institutes of Health Grant GM26788 (to D.R. and G.A.P.). Use of the Advanced Photon Source (APS) was supported by the U.S. Department of Energy, Basic Energy Sciences, Office of Science, under Contract No. W-31-109-Eng-38. Use of the BioCARS Sector 23 was supported by the National Institutes of Health, National Center for Research Resources, under Grant No. RR07707. We also thank the Stanford Synchrotron Radiation Laboratory (SSRL), a division of Stanford Linear Accelerator Center that is operated by Stanford University for the Department of Energy, for beamtime. SSRL is primarily supported by the DOE Offices of Basic Energy Sciences and Biological and Environmental Research, with additional support from the National Institutes of Health, National Center for Research Resources, Biomedical Technology Program, and the National Institute of General Medical Sciences.

[‡] The structural coordinates and structure factors have been deposited in the Protein Data Bank (PDB) as entry 2R2D.

* To whom correspondence should be addressed. W.F.: The University of Texas at Austin, College of Pharmacy, PHAR-MED CHEM, 1 University Station; A1935, Austin, TX 78712. Phone: (512) 232-4000. Fax: (512) 232-2606. E-mail: WaltFast@mail.utexas.edu. D.R.: Departments of Chemistry and Biochemistry and Rosenstiel Basic Medical Sciences Research Center, Brandeis University, Waltham, MA 02454-9110. E-mail: ringe@brandeis.edu.

[§] Brandeis University.

[||] These authors contributed equally.

[⊥] Division of Medicinal Chemistry.

[#] Graduate Program in Biochemistry.

[▽] Texas Institute for Drug and Diagnostic Development.

[1] Abbreviations: AHL, *N*-acyl-L-homoserine lactone; HSL, homoserine lactone; MBP, maltose binding protein; PCR, polymerase chain reaction; SDS, sodium dodecyl sulfate; PAGE, polyacrylamide gel electrophoresis; OD_{600}, optical density at 600 nm; ICP-MS, inductively coupled plasma mass spectrometry; *aiiB*, the gene for AHL lactonase; bp, base pairs; equiv, equivalents; TEV, tobacco etch virus; TB, Terrific Broth; MWCO, molecular weight cutoff; ESI-HRMS, electrospray ionization high resolution mass spectrometry; TLC, thin layer chromatography; mp, melting point; NMR, nuclear magnetic resonance; R_f, retention factor; mS milliSiemens; SAD, single-wavelength anomalous dispersion; rmsd, root mean square deviation.

10.1021/bi7012849 CCC: $37.00
Published on Web 09/28/2007

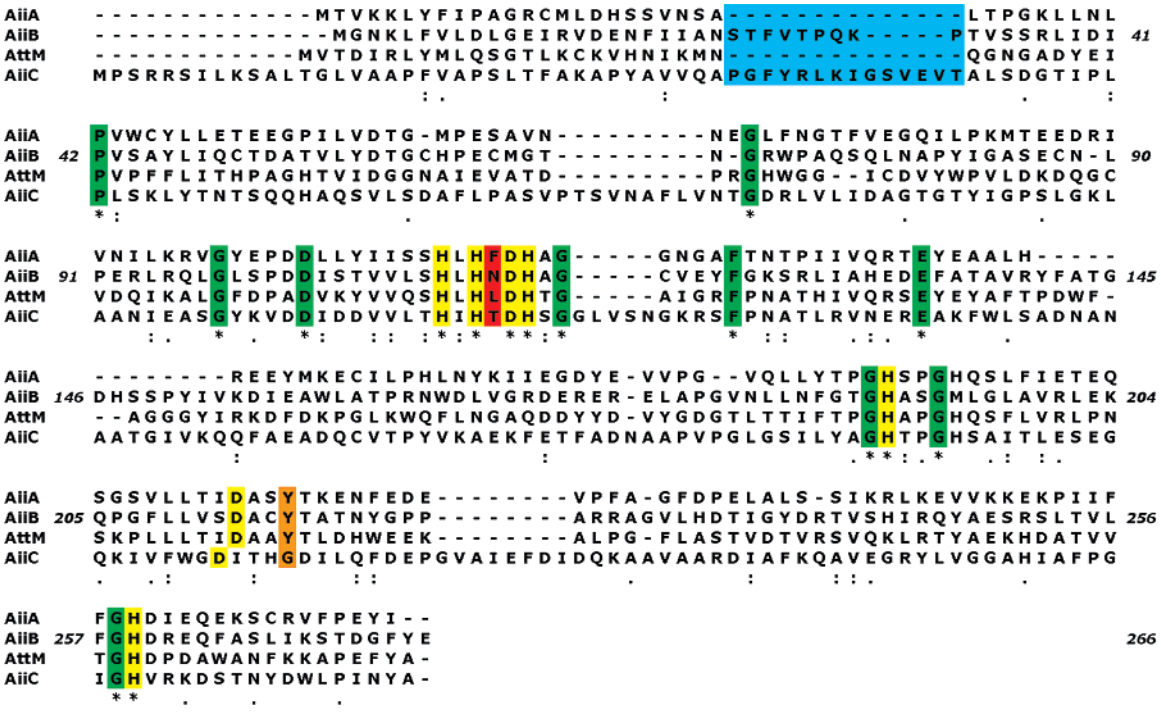

FIGURE 1: Sequence alignment of lactonases. Residues that coordinate to the zinc ions are highlighted in yellow. Other residues that are completely conserved are labeled in green. A sequence insert found in AiiB but not AiiA is highlighted in blue. The positions of two residues in the AiiB active site, Y216 and N114, are highlighted in orange and red, respectively. Beneath the alignments, * indicates identical residues, : indicates conservative substitutions, and . indicates semiconservative substitutions.

One bacterium known to produce both AHL signals and AHL lactonases is the plant pathogen *Agrobacterium tumefaciens*, which relies on *N*-(3-oxo-octanoyl)-L-homoserine lactone (3-oxo-C8-(*S*)-HSL) mediated quorum-sensing to regulate conjugal Ti plasmid transfer during plant infections (*11*). *A. tumefaciens* also carries three paralogues with significant sequence homology to AiiA: AiiB, AttM, and AiiC (*12*, *13*). The amino acid sequences of AiiA, AiiB, AttM, and AiiC (aligned using a online clustalW server (http://www.ch.embnet.org/index.html)) are shown in Figure 1. AiiB and AiiC were named for their sequence similarity to AiiA (*13*). AttM (*12*) was originally found in a gene region important for *A. tumefaciens* attachment to plant cells (*14*). Crude lysates of heterologously expressed AiiB and AttM have demonstrated their ability to hydrolyze AHLs (*13*). AiiC, however, lacks a tyrosine residue that is conserved in all other AHL lactonases (Figure 1) and is unable to hydrolyze various AHLs (*13*).

The AttM coding sequence is found within a gene cluster on the At plasmid of *A. tumefaciens*, and this enzyme has also been shown to be capable of degrading unsubstituted γ-butyrolactone (*13*, *15*, *16*). In wild type *A. tumefaciens*, expression of AttM appears to be growth-phase dependent, and is coordinated with a decrease in AHL concentration upon entering the stationary phase (*12*). This system has been cited as one of the first known examples of an AHL autoregulatory circuit, with the expression of AttM allowing *A. tumefaciens* to exit from the Ti plasmid conjugal transfer process (*12*). However, downstream genes in the *attM* cluster appear to only process metabolites of γ-butyrolactone and not the ring-opened metabolites of 3-oxo-C8-(*S*)-HSL (*16*), suggesting that regardless of AttM's physiological function in attenuating quorum-sensing, the operon does not appear to have evolved specifically to decompose and recycle AHLs (*17*).

In contrast, AiiB is found on the Ti plasmid of *A. tumefaciens* (*13*), the same plasmid that harbors *traI*, the biosynthetic gene for 3-oxo-C8-(*S*)-HSL, and *traR*, its cognate transcription factor, as well as most of the genes required for plant tumorigenesis (*17*). There has been little information reported about the regulation of AiiB expression, and the characterization of its specificity has been limited to only a few lactones using crude cell lysates (*13*). Here, we report the cloning, heterologous expression, purification, characterization, substrate specificity, and three-dimensional structure of AiiB. This report presents the second representative structure of a quorum-quenching AHL lactonase and the first that is derived from an organism that also uses AHL-dependent quorum-sensing pathways.

MATERIALS AND METHODS

Unless otherwise noted, all chemicals were obtained from Sigma-Aldrich Chemical Co. (St. Louis, MO) and all restriction enzymes were acquired from New England BioLabs (Beverly, MA). D_2O (99.9%) was purchased from Cambridge Isotope Laboratories (Andover, MA). Metal analysis of purified proteins was completed using inductively coupled plasma mass spectrometry as described previously (*18*).

Cloning and Expression. The coding sequence for the AHL lactonase AiiB was amplified from *A. tumefaciens* genomic DNA using specific end primers. The forward primer, 5′-GGTGGTTGCTCTTCCAACATGGGAAATAA-GCTGTTCGTTCTC-3′, contains a *Sap*I site (underlined). The reverse primer, 5′-GGTGGTCTGCAGTCATTATTCAT-AGAATCCGTCCGTGGATTTG-3′, contains a *Pst*I (underlined). The temperature program for the PCR was 5 min at 95 °C followed by 30 cycles of 30 s at 95 °C, 30 s at 55 °C, and 75 s at 72 °C. The resulting product was gel purified

(Qiaquick, Qiagen). Both the PCR product and the expression vector pTYB11 (New England BioLabs, Beverly, MA) were digested using restriction enzymes *Sap*I and *Pst*I. The resulting DNA fragments were purified, ligated together using T4 DNA ligase, and transformed into DH5αE *Escherichia coli* to produce an initial expression vector pTYB11-*aiiB*. The AiiB coding sequence (determined at the DNA Facility, University of Texas) was found to contain two nucleotide differences, T290C and G352A, from the reported sequence (*13*), but these are silent mutations and so were not corrected before protein expression tests. The AiiB coding sequence was later subcloned between the *Nde*I and *Xho*I restriction sites in the expression vector pET-27b, but this construct only yielded poor protein expression (data not shown). To construct a third expression vector, the temperature program described above and specific end primers were used to again amplify the AiiB coding sequence, using a forward primer, 5′-GCGCGGAAGGATTTCAATGGGAAATAAGCTGTTCGTTC-3′, which contains an *Xmn*I site (underlined), and a reverse primer, which contains a *Bam*HI site (underlined), 5′-GCGGATCCTTATTCATAGAATCCGTCCGTG-3. The product was cloned between the *Xmn*I and *Bam*HI sites of the pMAL-c2x-t-*aiiA* expression vector described earlier (*18*), after the starting vector had been digested and gel purified to remove its *aiiA* insert, resulting in the final expression vector pMAL-c2x-t-*aiiB*. In order to express AiiB with homogeneous metal content, an overnight culture of BL21(DE3) *E. coli* harboring the pMAL-c2x-t-*aiiB* expression plasmid was used to inoculate 2 × 1 L flasks of M9 minimal media containing ampicillin (100 μg/mL). The cultures were incubated with shaking at 37 °C until they reached an optical density (OD_{600nm}) of 0.6−0.7. To incorporate zinc, IPTG (0.5 mM) and $ZnSO_4$ (0.2 mM) were added along with fresh M9 media at the time of induction. To incorporate cobalt, IPTG (0.3 mM) and $CoCl_2$ (0.05 mM) were used instead. Protein production and cell harvesting were carried out as described previously (*4*).

Protein Purification and Metal Content Analysis. In order to maximize the yield of soluble AiiB protein derived from the pMAL-c2x-*aiiB* expression plasmid, cell pellets from induced cultures (2 L) were used immediately after harvesting. Ice-cold buffer (20 mM Tris-HCl, 100 mM NaCl, pH 7.4) was used to resuspend pelleted cells, which were subsequently lysed by sonication using a Fisher Scientific model 500 sonic dismembrator. The cell debris was removed as described previously (*18*). The resulting supernatant was loaded onto a DEAE-Sepharose FF column (2.5 cm × 20 cm) equilibrated with the same buffer as above, and excess proteins were washed from the column using additional buffer (200 mL). To elute bound proteins, the NaCl concentration was subsequently increased to 250 mM using a linear gradient. Fractions were analyzed by coomassie-stained SDS−PAGE, and those containing the maltose binding protein−AiiB fusion protein (MBP-AiiB) were found to generally elute at a conductivity near 19 mS/cm (approximately 190 mM NaCl). The fractions containing MBP-AiiB were pooled and further purified using an amylose-agarose column (2.5 cm × 10 cm) as described previously (*4*).

The MBP-AiiB fusion proteins, prepared with either $ZnSO_4$ or $CoCl_2$ supplements, were subsequently treated with tobacco etch virus (TEV) protease to remove the MBP tag, and the resulting untagged lactonase was purified as described previously using a DEAE-Sepharose fast flow column to remove the MBP fragment and TEV protease, and an amylose-agarose affinity column to remove trace amounts of uncleaved MBP-AiiB (*18*). The final protein was concentrated using an Amicon Ultra-15 (10 kDa MWCO) centrifugal filter device. Prior to use, trace metal ions in the filter were removed by soaking the filter cartridge in Tris-HCl (20 mM) buffer containing NaCl (5 mM) and *o*-phenanthroline (3 mM) at pH 7.0 for a few hours. This soak was followed by two rinses with the same buffer, each followed by centrifugation for 20 min at 3000*g*. After an additional overnight soak in the same buffer, the filter cartridges were extensively washed with metal-depleted water to remove any trace phenanthroline before they were used to concentrate AiiB. To determine the final metal content in AiiB, the concentrated protein and the eluate from the final concentration step were both analyzed by inductively coupled plasma mass spectrometry (ICP-MS; Department of Geological Sciences, The University of Texas at Austin). The trace metal ion concentrations of the eluate were subtracted from the metal ion concentrations in the AiiB sample, and the resulting sum was divided by the monomeric protein concentration to give the molar equivalents of metal ions bound to the purified protein.

Determining Steady-State Rate Constants for AHL Hydrolysis. To determine the substrate specificity of AiiB, five lactones were purchased (Sigma-Aldrich): *N*-butyryl-DL-homoserine lactone (C4-(*RS*)-HSL), *N*-(β-ketocaproyl)-DL-homoserine lactone (3-oxo-C6-(*RS*)-HSL), *N*-*t*-butyloxycarbonyl-DL-homoserine lactone (Boc-(*RS*)-HSL), *N*-carbobenzyloxy-L-homoserine lactone (CBZ-(*S*)-HSL), and γ-butyrolactone (GBL). Four additional lactones, *N*-hexanoyl-L-homoserine lactone (C6-(*S*)-HSL) (*18*), *N*-octanoyl-L-homoserine lactone (C8-(*S*)-HSL), *N*-(3-oxo-octanoyl)-L-homoserine lactone (3-oxo-C8-(*S*)-HSL), and *N*-decanoyl-L-homoserine lactone (C10-(*S*)-HSL) were synthesized as described below. The substrates' structures are shown below for easy reference. The steady-state rate constants for lactone hydrolysis as catalyzed by purified 2Zn-AiiB and 2Co-AiiB proteins were determined using a continuous spectrophotometric phenol red-based assay to detect proton release as described previously (*18*).

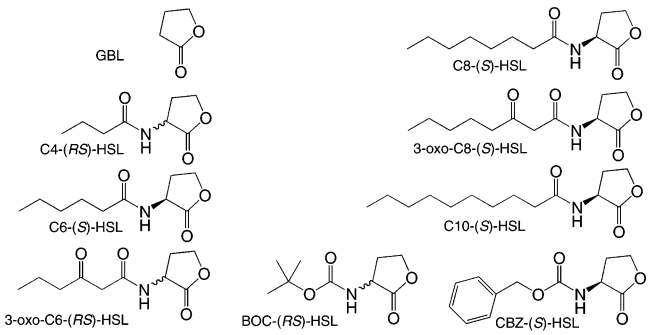

Synthesis of AHL Substrates. The substrate C8-(*S*)-HSL was synthesized using a procedure similar to that given by Chhabra et al. (*19*). Briefly, (*S*)-α-amino-γ-butyrolactone hydrobromide (5 mmol) was dissolved in ice-cold dimethylformamide (10 mL) with stirring. Triethylamine (11.5

mmole) was added. Subsequently, octanoyl chloride (7 mmol) was added dropwise, and the mixture was stirred at room temperature for 45 min. The solvent was removed by reduced-pressure rotary evaporation with mild heating (≤40 °C), and the resulting residue was dissolved in methylene chloride (40 mL). The organic layer was sequentially washed with sodium sulfate (1 M, pH 6, 3 × 40 mL) and saturated sodium chloride (1 × 40 mL) and dried using anhydrous magnesium sulfate. Solvent was removed by rotary evaporation at 20 °C. The compound was further purified by column chromatography on silica in ethyl acetate. Each fraction was analyzed by thin-layer chromatography (TLC), and fractions containing the desired compound were combined. The compound was obtained in a 90% yield: R_f = 0.6 in ethyl acetate; mp = 119−125 °C; ^{1}H NMR (300 MHz, $CDCl_3$) δ 0.84 (t, 3H), 1.25 (m, 8H), 1.61 (m, 2H), 2.15 (m, 2H), 2.22 (m, 1H), 2.8 (m, 1H), 4.26 (m, 1H), 4.44 (t, 1H), 4.58 (m, 1H), 6.21 (broad s, 1H); ^{13}C NMR (75 MHz, $CDCl_3$) δ 14.30, 22.83, 25.69, 29.21, 29.40, 30.76, 31.89, 36.41, 49.43, 66.38, 174.13, 175.96; EI-HRMS MH^+_{calc} = 227.3037, MH^+_{obs} = 228.1602; $[\alpha]^{20°C}_{D,methanol} = -24.7°$.

The substrate 3-oxo-C8-HSL was synthesized using a procedure similar to that of Schineller and Eberhard (*20*). Meldrum's acid (10 mmol) was added to anhydrous pyridine (10 mL) in a dry flask under $N_{2(g)}$ with stirring. Hexanoyl chloride (20 mmol) was added dropwise to the mixture on ice. The solution was allowed to react at room temperature for 1 h. (*S*)-α-Amino-γ-butyrolactone hydrobromide was added (10 mmol) and refluxed under $N_{2(g)}$ for 3 h. Solvent was removed by rotary evaporation with mild heating (≤40 °C), and the resulting residue was dissolved in ethyl acetate (100 mL) and decolorized with approximately 10 g of activated carbon. The compound was further purified by column chromatography on silica gel in hexanes (20%)/ethyl acetate (80%). Each fraction was analyzed by TLC, and fractions containing the desired compound were combined. Solvent was removed by rotary evaporation at 20 °C. The compound was obtained in a 33% yield: R_f = 0.4 in ethyl acetate; mp = 54−60 °C; ^{1}H NMR (300 MHz, $CDCl_3$) δ 0.84 (t, 3H), 1.23 (m, 4H), 1.5 (m, 2 H), 2.2 (m, 1H), 2.4 (m, 2 H), 2.6 (m, 1H), 3.5 (s, 2H), 4.2 (m, 1H), 4.4 (m, 1H), 4.6 (m, 1H), 7.7 (broad s, 1H); ^{13}C NMR (75 MHz, $CDCl_3$) δ 13.78, 22.28, 25.04, 29.47, 31.02, 35.98, 43.62, 48.97, 66.03, 166.49, 174.98, 206.31; EI-HRMS MH^+_{calc} = 241.2872, MH^+_{obs} = 242.1393; $[\alpha]^{20°C}_{D,methanol} = -20.3°$.

The substrate C10-(*S*)-HSL was synthesized in a manner similar to C8-(*S*)-HSL. Briefly, (*S*)-α-amino-γ-butyrolactone hydrobromide (5 mmol) was dissolved in ice-cold dimethylformamide (50 mL) with stirring. Triethylamine (12 mmole) was added, followed by the dropwise addition of decanoyl chloride (7 mmol). The solution was stirred at room temperature for 1.25 h. Solvent was removed by rotary evaporation with mild heating (≤55 °C). The resulting residue was dissolved in methylene chloride (100 mL), washed sequentially with sodium sulfate (1 M, pH 6, 2 × 50 mL) and saturated sodium chloride (1 × 50 mL), and dried using anhydrous magnesium sulfate. To afford further purification, the compound was recrystallized from a 50:50 (v/v) petroleum ether:ethyl acetate mixture: R_f = 0.6 in ethyl acetate; mp = 127−130 °C; ^{1}H NMR (300 MHz, $CDCl_3$) δ 0.85 (t, 3H), 1.24 (m, 12H), 1.62 (m, 2H), 2.10 (m, 1H), 2.22 (m, 2H), 2.8 (m, 1H), 4.27 (m, 1H), 4.44 (t, 1H), 4.53 (m, 1H), 6.07 (broad s, 1H); ^{13}C NMR (75 MHz, $CDCl_3$) δ 14.08, 22.63, 25.41, 29.28, 29.23, 29.29, 29.39, 30.63, 31.83, 36.17, 49.22, 66.10, 173.77, 175.59; EI-HRMS MH^+_{calc} = 255.3574, MH^+_{obs} = 256.1915; $[\alpha]^{20°C}_{D,methanol} = -23.5°$.

Crystallization, Data Collection, and Processing. The crystallization of AiiB protein was carried out in hanging drops by using standard screening kits (Hampton, San Diego), at room temperature. Crystals were obtained from a solution containing 35% glycerol and 0.26 M ammonium dihydrogen phosphate at an approximate pH of 3.5, which is the No. 3 condition in Hampton Crystal Screen Cryo. The AiiB protein also crystallizes without the presence of the glycerol. However, considering that glycerol can serve as a cryoprotectant, all crystals were grown and harvested in the presence of glycerol. The hanging drops were formed by mixing protein solution (10 mg/mL) with well solution at a volume ratio of 1:1.

A single-wavelength anomalous dispersion (SAD) data set was collected on beamline 23-IDD at GM/CA-CAT, Advance Photon Source (APS), Argonne National Laboratory. The wavelength used was 1.28 Å on the absorption edge of zinc. The SAD data set of 2.0 Å resolution was collected for 360 degrees with 0.5 degree oscillation per frame. Later a native data set was collected on beamline 9-1 at Stanford Synchrotron Radiation Laboratory (SSRL). The wavelength used was 0.99 Å to achieve the highest resolution possible. As a result, a data set with 1.75 Å resolution was collected with 1 degree oscillation per frame. Both data sets were integrated and scaled by using the HKL2000 software suite (*21*). Both data sets were indexed as space group *P*21 with 6 copies in an asymmetric unit.

Phasing, Model Building, Refinement, and Validation. The positions of the zinc ions were located from an anomalous difference Patterson synthesis calculated with the program SOLVE (*22*) using the SAD data set. During the Patterson calculation, data points beyond the resolution of 2.5 Å were left out due to the lack of anomalous signal at high resolution in the SAD data set. Preliminary phase angles were then calculated, and solvent flattening was carried out with the program RESOLVE (*23*, *24*). The autobuilt initial model from RESOLVE was used to start density-matching model building in the program COOT (*25*). The model refinement was carried out with the program REFMAC5 (*26*) in the CCP4 suite (*27*). Because there are 6 copies of the molecule in each asymmetric unit, the model building can be laborious. At the beginning of the model building, we only manually built one copy in an asymmetric unit. The other five copies were then found and generated with the molecular-replacement program PHASER (*28*). After the refinement in REFMAC5, the above process was repeated until the whole protein backbone was completely built. Once the protein backbone was completed, the structural model of all six copies was used as a single unit until the final completion of the model building. In each round of refinement in REFMAC5, the most recent structure model was taken through rigid body refinement, isotropic restrained refinement, and anisotropic restrained refinement (for the native data set). The model building and refinement were repeated till the lowest possible R_{free}/R_{cryst} values were reached. The

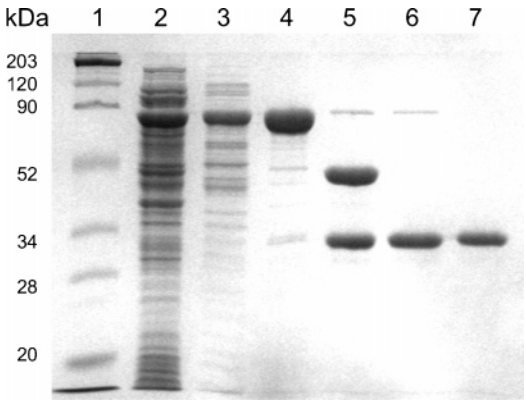

FIGURE 2: Purification of AHL lactonase AiiB. 12% SDS−PAGE denaturing protein gel showing proteins from (1) MW markers, (2) crude soluble extract, (3) eluate from DEAE anion-exchange column, (4) eluate from agarose affinity column, (5) after cleavage by TEV protease, (6) after DEAE chromatography, and (7) after amylose affinity chromatography.

program AREAIMOL (*29*) in the CCP4 software suite was used to calculate the surface area of the protein model.

The ligand coordinates file and topology file were generated with the DUNDEE server (http://davapc1.bioch.dundee.ac.uk/programs/prodrg/), and the program MONOSKETCHER in the CCP4 software suite. Structural graphic programs POVSCRIPT (*30*) and PYMOL (http://www.pymol.org) were used to generate all structural figures.

RESULTS

Cloning and Expression. The coding sequence for AiiB was initially amplified from *A. tumefaciens* genomic DNA and cloned into several different expression vectors. Initial sequencing revealed two silent mutations that were not corrected for in these studies. Only low yields of soluble active AiiB were obtained using either the pTYB11 or pET27b expression vectors. Previously, a pMAL-c2x-based expression vector was used successfully for expressing a similar AHL lactonase, AiiA, and was used here for the heterologous expression of soluble MBP-AiiB fusion protein (*18*). To incorporate zinc or cobalt into AiiB during expression, M9 minimal media, rather than TB media, was used to increase the homogeneity of the metal content. Because excess metal salts were found to decrease protein yield, optimal concentrations of $ZnSO_4$ (0.2 mM) and $CoCl_2$ (0.05 mM) supplements were determined experimentally.

Protein Purification and Metal Content Analysis. The untagged AiiB protein was purified to >95% purity as judged by coomassie-stained SDS−PAGE, by using several chromatographic steps (Figure 2). This untagged AiiB protein is predicted to contain 4 extra N-terminal amino acids, GRIS, that remain after cleavage of the MBP-AiiB fusion protein by TEV protease. This was confirmed experimentally by N-terminal protein sequencing (at the Protein Facility, University of Texas), which gave a sequence of GRISMGNKLFV. The yields of purified protein for 2Zn-AiiB and 2Co-AiiB were 13 mg and 6 mg per 2 L of expression culture, respectively. Using ICP-MS, the metal content of each purified protein was determined. The 2Zn-AiiB preparation contained 2.07 equiv of zinc, <0.01 equiv of cobalt, and 0.11 equiv of iron. The 2Co-AiiB preparation contained 1.5 equiv of cobalt, <0.01 equiv of zinc, and 0.05 equiv of iron.

Table 1: Steady-State Rate Constants for Lactone Hydrolysis by Dizinc AiiB

substrate	K_M (mM)	k_{cat} (s^{-1})	k_{cat}/K_M (M^{-1} s^{-1})
C4-(*RS*)-HSL	15 ± 1	5.8 ± 0.3	$3.9 \pm 0.5 \times 10^2$
C6-(*S*)-HSL	1.6 ± 0.2	24.8 ± 0.9	$1.6 \pm 0.3 \times 10^4$
3-oxo-C6-(*RS*)-HSL	4.6 ± 0.5	11.0 ± 0.4	$2.4 \pm 0.3 \times 10^3$
C8-(*S*)-HSL	1.0 ± 0.1	10.3 ± 0.2	$1.0 \pm 0.1 \times 10^4$
3-oxo-C8-(*S*)-HSL	2.5 ± 0.3	3.7 ± 0.1	$1.5 \pm 0.2 \times 10^3$
C10-(*S*)-HSL	0.11 ± 0.05	0.28 ± 0.08	$2.5 \pm 0.8 \times 10^3$
BOC-(*RS*)-HSL	7.7 ± 0.3	8.2 ± 0.1	$1.07 \pm 0.08 \times 10^3$
CBZ-(*S*)-HSL	0.77 ± 0.07	19.5 ± 0.6	$2.5 \pm 0.5 \times 10^4$
γ-butyrolactone (GBL)	340 ± 30	1.8 ± 0.1	5.3 ± 0.9

Table 2: Steady-State Rate Constants for Lactone Hydrolysis by Dicobalt AiiB

substrate	K_M (mM)	k_{cat} (s^{-1})	k_{cat}/K_M (M^{-1} s^{-1})
C6-(*S*)-HSL	5.9 ± 0.4	123 ± 3	$2.1 \pm 0.2 \times 10^4$
3-oxo-C6-(*RS*)-HSL	7.3 ± 0.9	34 ± 2	$5 \pm 1 \times 10^3$
3-oxo-C8-(*S*)-HSL	7.0 ± 0.8	37 ± 2	$5.3 \pm 0.9 \times 10^3$
CBZ-(*S*)-HSL	1.6 ± 0.1	55 ± 2	$3.4 \pm 0.3 \times 10^4$

Other metal ions were only found in trace amounts. Pretreatment of the Amicon filter cartridge with a metal chelator was essential to obtain purified protein that was homogeneously substituted with one type of metal ion.

Determining Steady-State Rate Constants for AHL Hydrolysis. Lactones with varying substitutions were assayed to determine their AiiB-catalyzed steady-state hydrolysis rates (Table 1). Typically, at least five different concentrations (from 0.1 to 5 × K_M) of each substrate were used to determine initial linear hydrolysis rates, which were then fit to the Michaelis−Menten equation using KaleidaGraph software (Synergy Software). The values for hydrolysis of C10-(*S*)-HSL should be considered an estimate because this substrate was not soluble enough to reach a concentration of 5 × K_M (concentrations ≥0.2 mM precipitate). The k_{cat}/K_M values for *N*-substituted homoserine lactones are of modest magnitude (10^2 to 10^4 M^{-1} s^{-1}) with a general preference shown for AHLs with acyl chains longer than four carbons. Commercially available racemic substrates have higher K_M values than pure (*S*)-enantiomers of similar length. Substrates with 3-oxo-substitutions were somewhat disfavored as substrates, reacting approximately 3- to 6-fold slower than substrates without this substitution (assuming that (*R*)-enantiomers do not interact with the enzyme). Surprisingly, homoserine lactones with the artificial *N*-protecting groups BOC and CBZ were substrates with k_{cat}/K_M values that rivaled naturally occurring AHLs. However, hydrolysis of the simplest lactone tested, γ-butyrolactone, was catalyzed several orders of magnitude slower than most AHLs. Previously, substitution of cobalt for zinc was shown to hyperactivate a homologous AHL lactonase from *B. thuringiensis*, AiiA (*4*). However, dicobalt substitution in AiiB only resulted in very minor increases (≤3.5-fold) of k_{cat}/K_M values for several different lactone substrates (Table 2). In summary, AiiB appers to function as a broad-specificity AHL lactonase.

Crystallization, Data Collection, and Processing. Crystals appeared overnight at room temperature (25 °C). The average size of the crystals is 0.3 mm x 0.2 mm x 0.1 mm with a rectangular shape. Despite the fact that the crystals are very thin in one of the three dimensions, they diffract to high

Table 3: Statistics of Structure Determination:

data set	SAD	native
resolution, Å	24.7−2.0	18.1−1.75
wavelength, Å	1.28	0.99
space group	*P*21	*P*21
cell dimensions		
a, *b*, *c*, Å	79.5, 157.9, 80.6	79.2, 158.0, 80.4
α, *β*, *γ*, deg	90.0, 104.4, 90.0	90.0, 104.5, 90.0
total reflections	407764	539428
unique reflections	118822	185201
completeness, %, overall (highest resolution bin)	94.5 (92.5)	96.6 (79.1)
average redundancies	3.4	2.9
linear R_{merge}, %, overall (highest resolution bin)	7.1 (46.5)	6.2 (60.6)
I/σ (I/σ_{cutoff})	13.1 (2.0)	16.6 (1.0)
R_{free}/R_{cryst}	23.8/17.6	21.5/16.4
rmsd bond, Å	0.02	0.01
rmsd angle, deg	1.9	1.5
average *B*, Å^2	33	30

resolutions with synchrotron radiation. A SAD data set with a 2.0 Å resolution and a native data set with 1.8 Å resolution were collected (Table 3). Both data sets were indexed as space group *P*21; they were integrated and scaled producing good statistics.

Phasing, Model Building, Refinement, and Validation. After calculating the anomalous patterson map in SOLVE, 12 peaks representing zinc ions were found in each asymmetric unit, corresponding to six molecules in each asymmetric unit of the primitive monoclinic space group (*P*21). After calculating the initial phase angles and carrying out solvent flattening in RESOLVE, an initial (incomplete) protein model was obtained. After model building with COOT and refinements with REFMAC5, all 276 amino acid residues were eventually built. The obtained structural model was then used for refinement with the native data set to 1.75 Å resolution.

DISCUSSION

Reagents that disrupt bacterial quorum-sensing have significant potential for controlling virulence factor production and biofilm formation in both clinical and industrial settings (*2*). Only a few types of quorum-quenching catalysts have been reported, and these have not been extensively characterized. To date, only one AHL lactonase, AiiA from *B. thuringiensis*, has been structurally characterized by X-ray crystallography (*8*, *9*). A search for homologous proteins in the *A. tumefaciens* genome revealed three paralogues, AiiB, AttM, and AiiC, which have significant amino acid sequence identity with AiiA (27%, 30%, and 19%, respectively) and less than 29% sequence identity with each other (*13*). Here we report the cloning, heterologous expression, purification, characterization, substrate specificity, and three-dimensional structure of AiiB, an AHL lactonase from *A. tumefaciens*.

Because AiiB is derived from an organism that produces 3-oxo-C8-HSL as a quorum-sensing molecule (*11*), it is of significant interest to see whether the AHL lactonases from *A. tumefaciens* show any specificity for, or against, this endogenous AHL. Here we use homogeneous purified AiiB to characterize steady-state hydrolysis rates of an unsubstituted lactone, *γ*-butyrolactone (GBL), and of AHLs with acyl chains from 4 to 10 carbons long (Table 1). The overall activity of 2Zn-AiiB is comparable (approximately 10-fold lower) to that of 2Zn-AiiA (*4*, *18*). AiiB prefers substrates with longer acyl chains, showing a 40-fold decrease in k_{cat}/K_M values between C6 and C4 acyl chains, and an additional 70-fold decrease for the unsubstituted GBL, which is a very poor substrate. The endogenous AHL of *A. tumefaciens*, 3-oxo-C8-(*S*)-HSL, is actually slightly disfavored and is hydrolyzed with a k_{cat}/K_M of $1.5 \pm 0.2 \times 10^3$ M^{-1} s^{-1}. In fact, substrates bearing 3-oxo-substituents are disfavored by 3 to 6-fold (assuming that (*R*)-enantiomers do not interact with the enzyme (*18*)). In sum, AiiB does not appear to have been evolved to specifically hydrolyze the endogenous AHL of *A. tumefaciens*, but instead is a broad-spectrum lactonase like those characterized from Gram-positive *Bacillus* species (which do not use AHL signaling). In addition, the endogenous 3-oxo-C8-(S)-HSL is not excluded as a substrate, suggesting that AiiB does not function by degrading foreign, but not endogenous, AHLs. Not much has been reported about the expression and regulation of AiiB in wild type *A. tumefaciens*, but unlike its paralogue AttM, AiiB does not appear to be upregulated in response to starvation signals or plant exudates (*13*, *15*, *16*, *31*). Notably, the broad specificity of AiiB is consistent with the previously proposed role of AHL lactonases in degrading AHLs of competing bacteria, thereby reducing competition for colonization of plant tissue during the initial stages of infection (*32*).

Crystallization of 2Zn-AiiB allowed a more detailed structural analysis of this catalyst. The monomer structure of AiiB shows an α*β*/*β*α fold similar to the zinc metallo-*β*-lactamase superfamily (Figure 3) (*33*). The first 170 residues of the protein form one domain of the monomer, while residues from 171 to 276 form the other. Similarities between monomer domains in other superfamily members have been used to propose that the overall α*β*/*β*α fold is derived from an ancient gene duplication during evolution (*33*), and the same can be proposed for AiiB. Although the sequence identity between domains is only 16%, they can be overlaid with a 4 Å rmsd over 72 residues using a secondary structure matching algorithm (*34*) (data not shown). AiiB is found to contain a dinuclear zinc binding site that is located in a loop-rich region on top of the two central *β* sheets. The axis of Zn1 and Zn2 is aligned with the interface of the two domains, and each contributes residues that serve as zinc ligands. Therefore, in addition to its role in lactone hydrolysis, the dinuclear metal center of AiiB may also provide significant stability to the overall protein structure. This is consistent with the observed importance of the metal center for protein folding in at least two other superfamily members (*4*, *35*).

The overall monomeric structure of AiiB is very similar to the other structurally characterized AHL lactonase, AiiA from *B. thuringiensis* (Figure 4) (*8*, *9*). Secondary structure matching (*34*) gives a 1.7 Å rmsd over 232 residues. However, the first half of the AiiB monomer, which is somewhat larger than the second, contains a sequence insert that is not present in the AiiA homologue. This sequence insert corresponds to nine extra residues, which are indicated in the sequence alignment (Figure 1) and comprise a loop region that links two extended *β*-strands and curves over the smaller second half of the monomer. This loop provides additional interactions between the two halves of the monomer that may help to maintain the overall α*β*/*β*α fold. This long loop is one of the most distinguishing structural

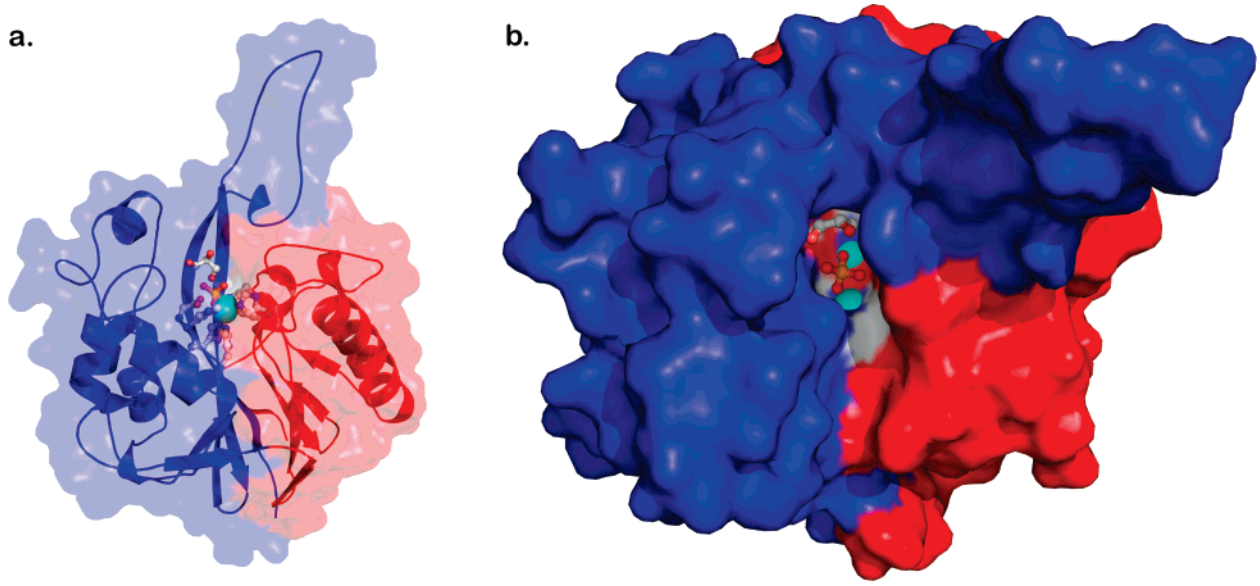

FIGURE 3: Overall structure of the AiiB monomer. Residues 1−170 are shown in blue, residues 171−276 in red. Zinc ions (Zn1 and Zn2) are shown as cyan spheres. A glycerol and a phosphate molecule are shown in ball and stick form and are colored according to atom types. (a) The monomer is in an orientation that places Zn2 behind Zn1. The surface feature of the protein is transparent so that the secondary structures are visible. Six zinc-binding residues are shown in ball and stick form and colored according to atom types. (b) The monomer is shown in an orientation that places Zn2 above Zn1.

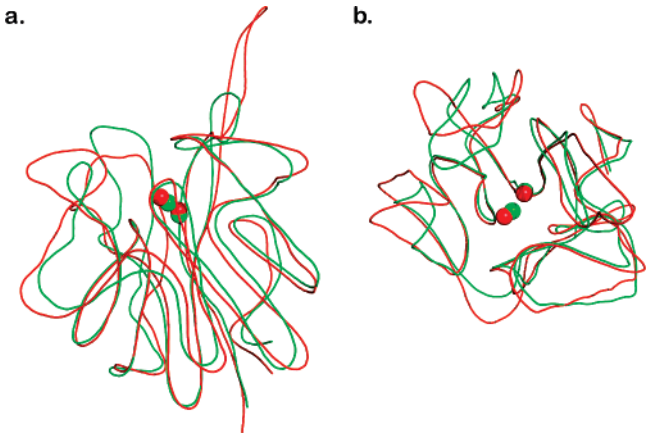

FIGURE 4: Comparison of overall structures of AiiB and AiiA. The protein backbones are shown as wires, zinc ions as spheres. AiiB is shown in red and AiiA in green. (a) A side view of the overlaid structures is shown. (b) A top view of the same comparison is depicted.

differences between AiiB and AiiA and is stabilized in an extended conformation through interactions made with the same residues in a separate monomer, forming a symmetrical crystallographic dimer (see below) (Figures 4 and 5). Other differences between AiiB and AiiA tend to occur in the helical or loop-rich regions, and not in the β sheet regions, which are almost structurally identical between these homologues.

In contrast to the monomeric AHL lactonase AiiA (*8*), evidence for a crystallographic dimer was observed for AiiB. Most of the observed protein−protein interactions are due to a symmetrical loop-to-loop interaction between residues Phe26 and Leu38 of each monomer, and an end-on helix interaction between the N-terminal ends (residues Asp233−Ile235) of the last α-helix found in each monomer (Figure 5). The loop-to-loop interaction roughly corresponds to the sequence insert found in AiiB (Phe26−Val34), that is missing in monomeric AiiA (Figure 1). Two monomers in the crystallographic dimer are related by a 2-fold symmetry axis, which is a characteristic of true (nonartifactual) dimers. The computer program AREAIMOL in the CCP4 suite was used to calculate the solvent accessible surface areas (ASA) for both the monomer and the crystallographic dimer of AiiB. The difference of ASA between two monomers and the dimer (ΔASA) is 2055 Å^2, which represents a buried surface area of 1028 Å^2 for each monomer. A ΔASA range of 368−4746 Å^2 is considered to be a reasonable area for formation of a functional dimer (*36*), suggesting that the crystallographic AiiB dimer may represent a functional solution-phase dimer. The crystallographic AiiB dimer is formed in such a way that neither of the active sites has been blocked, and that contributions from both monomers could possibly play a role in forming an extended substrate binding pocket. Studies to determine the importance of this loop-to-loop interaction to AiiB oligomerization, the oligomeric state in solution (at neutral pH), and its possible contributions to the enzyme's activity and specificity are currently underway. In the metallo-β-lactamase superfamily, there are known examples of monomers (*33*), dimers (*37*), and tetramers (*38*). However the protein−protein interactions used to mediate oligimerization are absent in AiiA, are not like those seen in AiiB, are quite different between each known example, and therefore, appear to have evolved independently several times within this superfamily.

The dinuclear zinc site is adjacent to a cavity in the middle of the protein, which presumably comprises the active site cavity of AiiB (Figure 3b). The homologous protein AiiA has a large branched cavity (*8*). In comparison, the AiiB active site cavity is not as large and is not branched, which provides additional constraints to be considered when proposing a substrate-binding model. Extending from the active site cavity along the Zn2-to-Zn1 axis is a long groove on the surface of the protein formed at the interface between the two halves of the monomer (Figure 3b). The extended groove may provide a binding site for varying length *N*-acyl

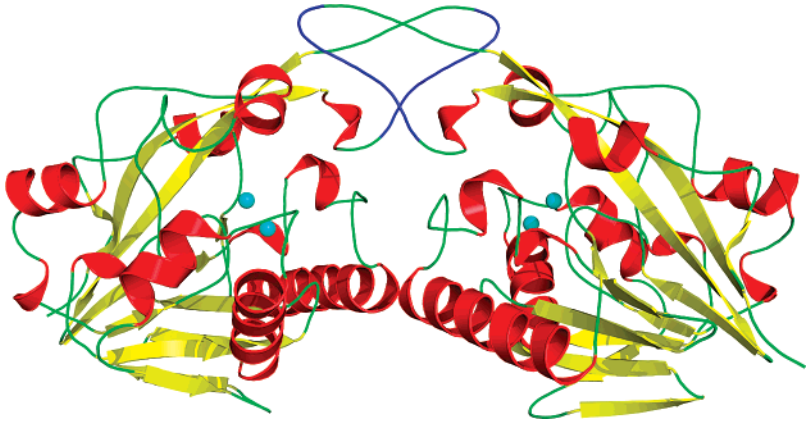

FIGURE 5: The crystallographic dimer of AiiB. Residues corresponding to the "extra loop" noted in the sequence alignments of AiiA and AiiB (Figure 1) are shown in blue, and the rest of the dimer is colored according to secondary structure. Zinc ions in the active sites are shown as cyan spheres.

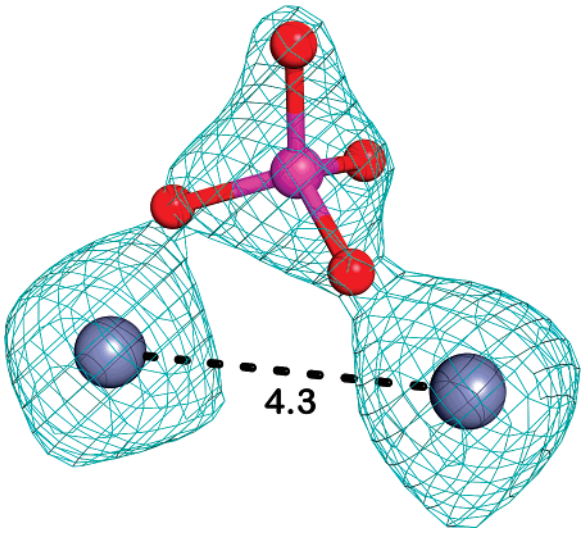

FIGURE 6: Identification of a phosphate bound between two zinc ions. Two zinc ions are shown as silver spheres. The modeled phosphate ion is shown in ball-and-stick form with oxygen atoms in red and the phosphorus in magenta. The electron density ($2F_o - F_c$ map) is show as a green mesh at a contour level of 4.0σ. The long distance (4.3 Å) between the two zinc ions is labeled in angstroms.

chains of the AHL substrates. Although structural and functional studies will be required to verify this proposed substrate-binding groove, the related metallo-β-lactamases are known to have similar shallow surface grooves with significant plasticity, which enable these catalysts to bind structurally diverse substrates (*39*). However, flexible substrate-binding flaps like those seen in some metallo-β-lactamases (*40*, *41*) are not readily identifiable in the currently known AHL lactonase structures.

The active-site cavity contains water and a glycerol molecule from the crystallization buffer (Figure 3b). Notably, a strong electron density peak was observed between the two zinc ions. This peak is too strong to be modeled as a bridging water or a hydroxide molecule, as was observed in the AiiA homologue (*8*, *9*). Therefore, considering the abundance of phosphate in the crystallization condition (0.26 M), the density was modeled as phosphate ion and it refines well (Figure 6). The phosphate forms bidentate coordination bonds with the dinuclear zinc site, with separate oxygens coordinating to each zinc ion, resulting in a three-centered bridge instead of the shorter hydroxide bridge observed in AiiA (*8*, *9*). The resulting distance between Zn1 and Zn2 is 4.3 Å in our structural model. According to the previous structures of AiiA (*8*, *9*) and previous reviews of other dinuclear zinc enzymes (*42*, *43*), Zn1−Zn2 distances are usually in the range of 3.5−4.4 Å. Although the long Zn1−Zn2 distance in AiiB is probably the result of substituting the phosphate for the smaller hydroxide bridge, it may also illustrate the ability of this flexible dizinc site to accommodate differently coordinated reaction intermediates (*44*). Coordination bridges of variable length have also been seen with the unrelated dinuclear aminopeptidase from *Aeromonas proteolytica*, which is able to expand the length of a bridge from 1 (a hydroxide) to 3 (a phosphonic acid) depending on the bound ligand (*45*, *46*).

The primary coordination ligands of the dinuclear zinc site show similarities to the AiiA homologue, but there are some notable differences. Zn1 is five coordinate with a slightly distorted trigonal bipyrimidal coordination geometry (*47*). Three histidines (H111, H113, and H191) contribute as primary ligands along with one oxygen from the bound phosphate, and one oxygen atom of D213, which also bridges the dinuclear site. This is very similar to the Zn1 geometry observed in the structure of AiiA (*8*, *9*). In contrast, Zn2 also has five ligands, but has a coordination geometry closer to a distorted square pyrimad (*47*) rather than the distorted trigonal bipyrimidal geometry observed in the AiiA structure. The primary ligands of Zn2 are monodentate interactions with H116, H259, and one of the oxygens from the bridging phosphate. In addition, both oxygens of D213 are ligands to Zn2 and bind in a bidentate fashion, with one of these oxygens also bridging between the two zinc ions. Notably, D115, a completely conserved residue that serves as a Zn2 ligand in the AiiA homologue (*8*, *9*), is not a zinc ligand in AiiB (Figure 7). The closest oxygen atom of D115 is 3.4 Å away from Zn2, which is too far to serve as an effective Zn2 ligand. This may be a result of protonation of D115 at the low pH (3.5) of the crystallization conditions. A similar detachment from Zn2 of a structurally homologous protonated Asp residue found in a related metallo-β-lactamase was also observed when crystallized under acidic conditions (*48*).

One of the two noncoordinating phosphate oxygens is within hydrogen-bonding distances of the side chains of

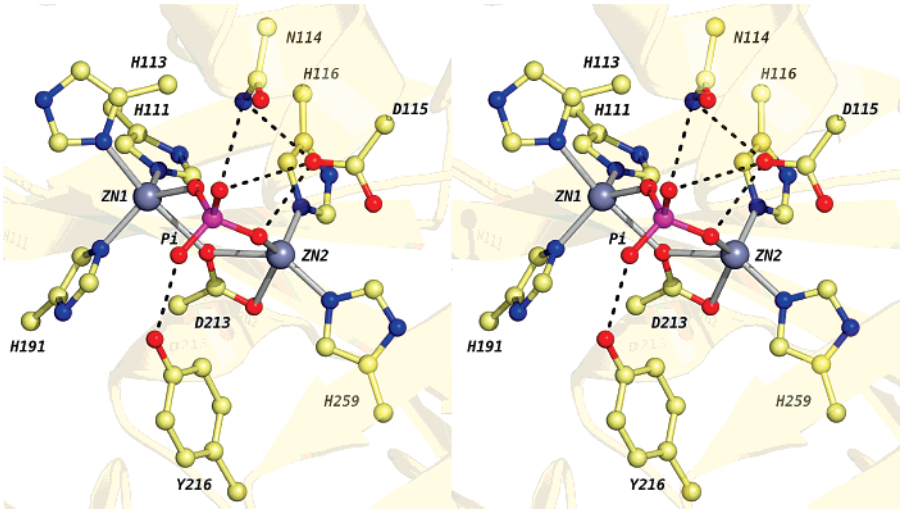

FIGURE 7: Stereoview of the AiiB active site. All active site residues and the phosphate (Pi) are shown in ball-and-stick form. The zinc ions (Zn1 and Zn2) are shown as silver spheres. The carbon atoms are colored in a pale yellow, nitrogen atoms in blue, oxygen atoms in red, and the phosphorus atom in magenta. Coordination bonds to the zinc ions are shown as silver sticks. The key hydrogen bonds formed between the phosphate and potential catalytic residues are shown as dashed lines (see Figure 9a for distance measurements).

residues N114 and D115, which are also in H-bonding distance with each other. Therefore, this phosphate oxygen is most likely protonated, a reasonable proposal considering the pK_a values of phosphate and the pH of the crystallization conditions. It is possible that N114 plays some role in the catalytic mechanism of AiiB. However, N114 is not conserved either in the AHL lactonases or in the metallo-β-lactamase superfamily, suggesting that it probably does not play a major role in catalysis. For example, the homologue AiiA places a phenylalanine in the equivalent position (Figure 1).

The second noncoordinating oxygen of the phosphate is within hydrogen-bonding distance of the phenol oxygen of Y216. This residue, while not conserved across the metallo-β-lactamase superfamily, is absolutely conserved within the AHL lactonase family of enzymes. Mutations at this position have been shown to be detrimental to activity (*9*, *49*), and the Y216 phenol has been postulated to either stabilize a tetrahedral intermediate (*8*) or act as a general acid to protonate the lactone's leaving group oxygen (*8*, *9*). In the AiiB structure, the phenol of Y216 appears to stabilize the tetrahedral phosphate ligand that is bound to the dinuclear zinc site (Figure 7). The *A. tumefaciens* paralogue AiiC does not have this conserved tyrosine (Figure 1), and also lacks AHL lactonase activity (*13*).

In comparison to the active site of the homologous lactonase AiiA, the AiiB metal-binding site is quite similar (Figure 8), with the notable differences being a longer Zn−Zn distance, the substitution of phosphate for the bridging hydroxide, substitution of N114 for Phe107, and the detached D115 which no longer serves as a Zn2 ligand (vide infra). It is interesting to note that the position of Zn2 is conserved despite significant changes in coordination, and that the longer Zn−Zn distance is achieved by a repositioning of Zn1 with the conserved histidine (and D213) residues "tracking" along with this movement. Zn−Zn repositioning in related metallo-β-lactamase enzymes has also been observed, but repositioning of Zn2 rather than Zn1 is usually seen (*48*). This difference may be a consequence of the extra bridge formed by D213 between the zinc atoms in AHL lactonases that is absent in metallo-β-lactamase.

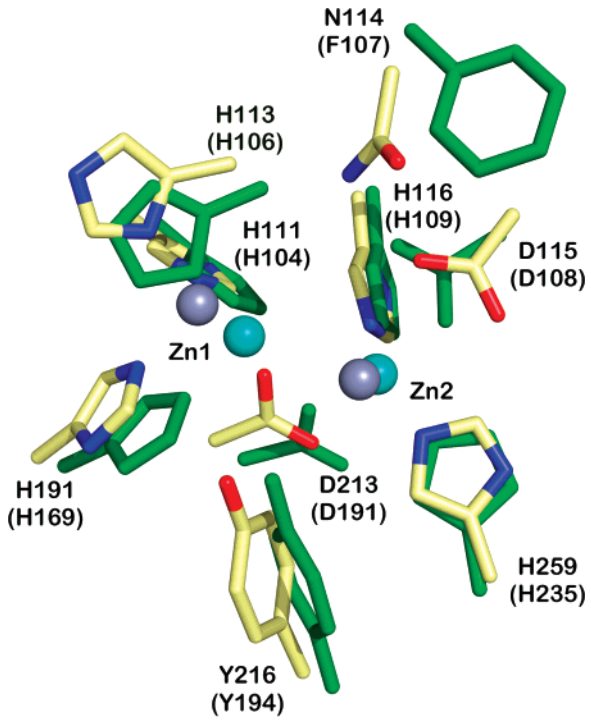

FIGURE 8: Structural comparison between the active sites of AiiA and AiiB. All active site residues are shown as sticks, and zinc ions as spheres. Residues from AiiB are colored according to atom types: with carbon atoms in pale yellow, nitrogen atoms in blue, oxygen atoms in red, and zinc ions in silver. All residues from AiiA are shown in green, and two zinc ions from AiiA are in cyan. Residues from AiiA are labeled in parentheses under their equivalent residues in AiiB.

Although further experimentation will be required, the phosphate-bound AiiB structure provides some possible insight into the catalytic mechanism of AHL lactonases. The smaller active site cavity and the putative substrate binding groove suggest a likely substrate orientation that places the acyl chain along the seam between domains, with the lactone's carbonyl over Zn1, and the leaving group oxygen over Zn2. This proposed orientation is opposite to that proposed by Kim et al., which reverses the lactone orientation relative to each zinc (*9*). However our proposal is consistent

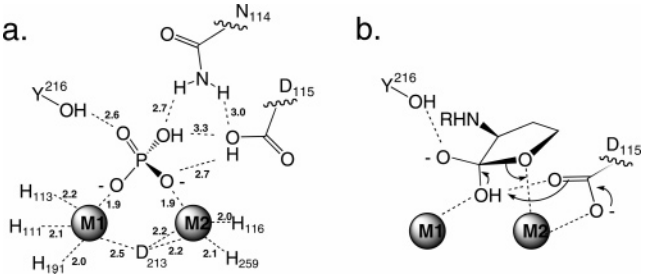

FIGURE 9: (a) Proposed hydrogen-bonding patterns in the 2Zn-AiiB complex with the HPO_4^{2-} dianion. Distances between heteroatoms are shown in angstroms. (b) Proposed tetrahedral adduct formed during AHL hydrolysis based on the interactions observed for binding the tetrahedral HPO_4^{2-} dianion and the proposed substrate orientation described in the text, en route to formation of a metal-bound intermediate as proposed in ref (*4*).

with substrate placement observed in the rest of the metallo-β-lactamase superfamily, which places the substrate's carbonyl oxygen over Zn1 and leaving group heteroatom over Zn2 (*40*, *50*). The ability of the conserved Y216 to stabilize a tetrahedral species (HPO_4^{2-}) bound to the dinuclear metal site immediately suggests that it may stabilize a tetrahedral adduct formed during the first step of lactone hydrolysis (Figure 9). Semiquantitative analysis of a tyrosine mutant in AiiA only shows a 3-fold reduction in activity (*9*), but the full effect of this mutation could be masked by a subsequent slower step. Therefore, a more detailed kinetic analysis of this mutation is required for meaningful interpretation. Alternatively, the role of Y216 as a general acid to protonate the leaving group has been suggested (*8*, *9*), although the high pK_a expected for a tyrosine phenol (*ca.* 10) would seem to disfavor this mechanism. A more likely proposal for a proton shuttle may be D115, which is hydrogen bonded to the bridging hydroxide in AiiA (presumably the catalytic nucleophile) but is protonated and repositioned to hydrogen bond with Zn2-bound HPO_4^{2-} oxygen atom in the AiiB structure. Surprisingly, this repositioning appears to occur without significant alteration of the Zn2 location. This makes D115 a good candidate for a proton shuttle because its different protonation forms relocate to positions relevant to catalyzing lactone hydrolysis without causing significant perturbations in the rest of the active site. Although not uniformly accepted, a similar role has been proposed for the structurally homologous aspartate residue in some metallo-β-lactamases and in the unrelated dinuclear isoaspartyl dipeptidase (*40*, *51*, *52*).

In summary, dinuclear zinc AiiB appears to act as a broad specificity AHL lactonase and this detailed structural analysis provides the first glimpse of a quorum-quenching protein derived from an organism that also uses AHLs as signaling molecules. This information should greatly facilitate mechanistic studies of related quorum-quenching catalysts and should also accelerate the development of effective reagents for preventing quorum-sensing regulated processes in a variety of Gram-negative bacteria.

ACKNOWLEDGMENT

We thank Sonal Tuljapurkar and Helena Bianchi for their help in the initial cloning of the AiiB coding sequence. We thank the whole GM/CA-CAT staff for help and support during data collection, and Dr. Jose Manuel Martinez Caaveiro for assistance with figure preparation.

REFERENCES

1. Parsek, M. R., and Greenberg, E. P. (2000) Acyl-homoserine lactone quorum sensing in gram-negative bacteria: a signaling mechanism involved in associations with higher organisms, *Proc. Natl. Acad. Sci. U.S.A. 97*, 8789−8793.
2. Dong, Y. H., Wang, L. H., and Zhang, L. H. (2007) Quorum-quenching microbial infections: mechanisms and implications, *Philos. Trans. R. Soc. London, Ser. B: Biol. Sci. 362*, 1201−1211.
3. Dong, Y. H., Xu, J. L., Li, X. Z., and Zhang, L. H. (2000) AiiA, an enzyme that inactivates the acylhomoserine lactone quorum-sensing signal and attenuates the virulence of *Erwinia carotovora*, *Proc. Natl. Acad. Sci. U.S.A. 97*, 3526−3531.
4. Momb, J., Thomas, P. W., Breece, R. M., Tierney, D. L., and Fast, W. (2006) The quorum-quenching metallo-gamma-lactonase from *Bacillus thuringiensis* exhibits a leaving group thio effect, *Biochemistry 45*, 13385−13393.
5. Afriat, L., Roodveldt, C., Manco, G., and Tawfik, D. S. (2006) The latent promiscuity of newly identified microbial lactonases is linked to a recently diverged phosphotriesterase, *Biochemistry 45*, 13677−13686.
6. Draganov, D. I., Teiber, J. F., Speelman, A., Osawa, Y., Sunahara, R., and La Du, B. N. (2005) Human paraoxonases (PON1, PON2, and PON3) are lactonases with overlapping and distinct substrate specificities, *J. Lipid Res. 46*, 1239−1247.
7. Daiyasu, H., Osaka, K., Ishino, Y., and Toh, H. (2001) Expansion of the zinc metallo-hydrolase family of the beta-lactamase fold, *FEBS Lett. 503*, 1−6.
8. Liu, D., Lepore, B. W., Petsko, G. A., Thomas, P. W., Stone, E. M., Fast, W., and Ringe, D. (2005) Three-dimensional structure of the quorum-quenching N-acyl homoserine lactone hydrolase from *Bacillus thuringiensis*, *Proc. Natl. Acad. Sci. U.S.A. 102*, 11882−11887.
9. Kim, M. H., Choi, W. C., Kang, H. O., Lee, J. S., Kang, B. S., Kim, K. J., Derewenda, Z. S., Oh, T. K., Lee, C. H., and Lee, J. K. (2005) The molecular structure and catalytic mechanism of a quorum-quenching N-acyl-L-homoserine lactone hydrolase, *Proc. Natl. Acad. Sci. U.S.A. 102*, 17606−17611.
10. Zhou, Y., Ye, W.-x., Zhou, Y., Zhu, C.-g., Sun, M., and Yu, Z.-n. (2006) Ethanol tolerance, yield of melanin, swarming motility and growth are correlated with the expression levels of *aiiA* gene in *Bacillus thuringiensis*, *Enzyme Microb. Technol. 38*, 967−974.
11. Zhang, L., Murphy, P. J., Kerr, A., and Tate, M. E. (1993) *Agrobacterium* conjugation and gene regulation by N-acyl-L-homoserine lactones, *Nature 362*, 446−448.
12. Zhang, H. B., Wang, L. H., and Zhang, L. H. (2002) Genetic control of quorum-sensing signal turnover in *Agrobacterium tumefaciens*, *Proc. Natl. Acad. Sci. U.S.A. 99*, 4638−4643.
13. Carlier, A., Uroz, S., Smadja, B., Fray, R., Latour, X., Dessaux, Y., and Faure, D. (2003) The Ti plasmid of *Agrobacterium tumefaciens* harbors an *attM*-paralogous gene, *aiiB*, also encoding N-Acyl homoserine lactonase activity, *Appl. Environ. Microbiol. 69*, 4989−4993.
14. Matthysse, A. G., Yarnall, H., Boles, S. B., and McMahan, S. (2000) A region of the *Agrobacterium tumefaciens* chromosome containing genes required for virulence and attachment to host cells, *Biochim. Biophys. Acta 1490*, 208−212.
15. Carlier, A., Chevrot, R., Dessaux, Y., and Faure, D. (2004) The assimilation of gamma-butyrolactone in *Agrobacterium tumefaciens* C58 interferes with the accumulation of the N-acyl-homoserine lactone signal, *Mol. Plant Microbe Interact. 17*, 951−957.
16. Chai, Y., Tsai, C. S., Cho, H., and Winans, S. C. (2007) Reconstitution of the Biochemical Activities of the AttJ Repressor and the AttK, AttL, and AttM Catabolic Enzymes of *Agrobacterium tumefaciens*, *J. Bacteriol 189*, 3674−3679.
17. White, C. E., and Winans, S. C. (2007) Cell-cell communication in the plant pathogen *Agrobacterium tumefaciens*, *Philos. Trans. R. Soc. London, Ser. B: Biol. Sci. 362*, 1135−1148.
18. Thomas, P. W., Stone, E. M., Costello, A. L., Tierney, D. L., and Fast, W. (2005) The Quorum-Quenching Lactonase from *Bacillus thuringiensis* Is a Metalloprotein, *Biochemistry 44*, 7559−7569.

19. Chhabra, S. R., Harty, C., Hooi, D. S., Daykin, M., Williams, P., Telford, G., Pritchard, D. I., and Bycroft, B. W. (2003) Synthetic analogues of the bacterial signal (quorum sensing) molecule N-(3-oxododecanoyl)-L-homoserine lactone as immune modulators, *J. Med. Chem. 46*, 97−104.
20. Eberhard, A., and Schineller, J. B. (2000) Chemical synthesis of bacterial autoinducers and analogs, *Methods Enzymol. 305*, 301−315.
21. Otwinowski, Z., and Minor, W. (1997) Processing of X-ray diffraction data collected in oscillation mode, *Methods Enzymol. 276*, 307−326.
22. Terwilliger, T. C., and Berendzen, J. (1999) Automated MAD and MIR structure solution, *Acta Crystallogr. D 55*, 849−861.
23. Terwilliger, T. C. (2000) Maximum-likelihood density modification, *Acta Crystallogr. D 56*, 965−972.
24. Terwilliger, T. C. (2002) Automated main-chain model building by template matching and iterative fragment extension, *Acta Crystallogr. D 59*, 38−44.
25. Emsley, P., and Cowtan, K. (2004) Coot: model-building tools for molecular graphics, *Acta Crystallogr., Sect. D: Biol. Crystallogr. 60*, 2126−2132.
26. Murshudov, G. N., Vagin, A., and Dodson, J. (1997) Refinement of macromolecular structures by the maximum-likelihood method, *Acta Crystallogr. D 53*, 240−255.
27. Collaborative, Computational, Project, No. 4 (1994) The CCP4suite: programs for protein crystallography, *Acta Crystallogr. D 50*, 760−763.
28. Read, R. J. (2001) Pushing the boundaries of molecular replacement with maximum likelihood, *Acta Crystallogr. D 57*, 1373−1382.
29. Lee, B., and Richards, F. M. (1971) The interpretation of protein structure: Estimation of static accessibility, *J. Mol. Biol. 55*, 379−400.
30. Fenn, T. D., Ringe, D., and Petsko, G. A. (2003) POVScript+: a program for model and data visualization using persistence of vision ray-tracing, *J. Appl. Crystallogr. 36*, 944−947.
31. Zhang, H. B., Wang, C., and Zhang, L. H. (2004) The quormone degradation system of *Agrobacterium tumefaciens* is regulated by starvation signal and stress alarmone (p)ppGpp, *Mol. Microbiol. 52*, 1389−1401.
32. Chevrot, R., Rosen, R., Haudecoeur, E., Cirou, A., Shelp, B. J., Ron, E., and Faure, D. (2006) GABA controls the level of quorum-sensing signal in *Agrobacterium tumefaciens*, *Proc. Natl. Acad. Sci. U.S.A. 103*, 7460−7464.
33. Carfi, A., Pares, S., Duee, E., Galleni, M., Duez, C., Frere, J. M., and Dideberg, O. (1995) The 3-D structure of a zinc metallo-beta-lactamase from *Bacillus cereus* reveals a new type of protein fold, *EMBO J. 14*, 4914−4921.
34. Krissinel, E., and Henrick, K. (2004) Secondary-structure matching (SSM), a new tool for fast protein structure alignment in three dimensions, *Acta Crystallogr., Sect. D: Biol. Crystallogr. 60*, 2256−2268.
35. Periyannan, G., Shaw, P. J., Sigdel, T., and Crowder, M. W. (2004) In vivo folding of recombinant metallo-beta-lactamase L1 requires the presence of Zn(II), *Protein Sci. 13*, 2236−2243.
36. Jones, S., and Thornton, J. M. (1996) Principles of protein-protein interactions, *Proc. Natl. Acad. Sci. U.S.A. 93*, 13−20.
37. Ishii, R., Minagawa, A., Takaku, H., Takagi, M., Nashimoto, M., and Yokoyama, S. (2005) Crystal structure of the tRNA 3′ processing endoribonuclease tRNase Z from *Thermotoga maritime*, *J. Biol. Chem. 280*, 14138−14144.
38. Ullah, J. H., Walsh, T. R., Taylor, I. A., Emery, D. C., Verma, C. S., Gamblin, S. J., and Spencer, J. (1998) The crystal structure of the L1 metallo-beta-lactamase from *Stenotrophomonas maltophilia* at 1.7 Å resolution, *J. Mol. Biol. 284*, 125−136.
39. Scrofani, S. D., Chung, J., Huntley, J. J., Benkovic, S. J., Wright, P. E., and Dyson, H. J. (1999) NMR characterization of the metallo-beta-lactamase from *Bacteroides fragilis* and its interaction with a tight-binding inhibitor: role of an active-site loop, *Biochemistry 38*, 14507−14514.
40. Crowder, M. W., Spencer, J., and Vila, A. J. (2006) Metallo-beta-lactamases: novel weaponry for antibiotic resistance in bacteria, *Acc. Chem. Res. 39*, 721−728.
41. Huntley, J. J., Fast, W., Benkovic, S. J., Wright, P. E., and Dyson, H. J. (2003) Role of a solvent-exposed tryptophan in the recognition and binding of antibiotic substrates for a metallo-beta-lactamase, *Protein Sci. 12*, 1368−1375.
42. Wang, Z., Fast, W., Valentine, A. M., and Benkovic, S. J. (1999) Metallo-beta-lactamase: structure and mechanism, *Curr. Opin. Chem. Biol. 3*, 614−622.
43. Auld, D. S. (2001) Zinc coordination sphere in biochemical zinc sites, *Biometals 14*, 271−313.
44. Lavie, A., Allen, K. N., Petsko, G. A., and Ringe, D. (1994) X-ray crystallographic structures of D-xylose isomerase-substrate complexes position the substrate and provide evidence for metal movement during catalysis, *Biochemistry 33*, 5469−5480.
45. Desmarais, W., Bienvenue, D. L., Bzymek, K. P., Petsko, G. A., Ringe, D., and Holz, R. C. (2006) The high-resolution structures of the neutral and the low pH crystals of aminopeptidase from *Aeromonas proteolytica*, *J. Biol. Inorg. Chem. 11*, 398−408.
46. Stamper, C., Bennett, B., Edwards, T., Holz, R. C., Ringe, D., and Petsko, G. (2001) Inhibition of the aminopeptidase from *Aeromonas proteolytica* by L-leucinephosphonic acid. Spectroscopic and crystallographic characterization of the transition state of peptide hydrolysis, *Biochemistry 40*, 7035−7046.
47. Muetterties, E. L., and Guggenberger, L. J. (1974) Idealized Polytopal Forms. Description of Real Molecules Referenced to idealized Polygons or Polyhedra in Geometric Reaction Path Form, *J. Am. Chem. Soc. 96*, 1748−1756.
48. Davies, A. M., Rasia, R. M., Vila, A. J., Sutton, B. J., and Fabiane, S. M. (2005) Effect of pH on the active site of an Arg121Cys mutant of the metallo-beta-lactamase from *Bacillus cereus*: implications for the enzyme mechanism, *Biochemistry 44*, 4841−4849.
49. Lu, X., Yuan, Y., Xue, X. L., Zhang, G. P., and Zhou, S. N. (2006) Identification of the critical role of Tyr-194 in the catalytic activity of a novel N-acyl-homoserine lactonase from marine *Bacillus cereus* strain Y2, *Curr. Microbiol. 53*, 346−350.
50. Cameron, A. D., Ridderstrom, M., Olin, B., and Mannervik, B. (1999) Crystal structure of human glyoxalase II and its complex with a glutathione thiolester substrate analogue, *Struct. Fold. Des. 7*, 1067−1078.
51. Marti-Arbona, R., Fresquet, V., Thoden, J. B., Davis, M. L., Holden, H. M., and Raushel, F. M. (2005) Mechanism of the reaction catalyzed by isoaspartyl dipeptidase from *Escherichia coli*, *Biochemistry 44*, 7115−7124.
52. Llarrull, L. I., Fabiane, S. M., Kowalski, J. M., Bennett, B., Sutton, B. J., and Vila, A. J. (2007) Asp120 locates Zn2 for optimal metallo-beta-lactamase activity, *J. Biol. Chem. 282*, 18276−18285.

BI7012849